SANDIA REPORT

SAND2014-17329
Unlimited Release
Printed September 2014

Thermal Characterization and Properties of a Copper-Diamond Composite

Pin Yang, Christopher B. DiAntonio, Tom Chavez, and Eric N. Coker

Prepared by
Sandia National Laboratories
Albuquerque, New Mexico 87185 and Livermore, California 94550

Sandia National Laboratories is a multi-program laboratory managed and operated by Sandia Corporation, a wholly owned subsidiary of Lockheed Martin Corporation, for the U.S. Department of Energy's National Nuclear Security Administration under contract DE-AC04-94AL85000.

Issued by Sandia National Laboratories, operated for the United States Department of Energy by Sandia Corporation.

Available to DOE and DOE contractors from
U.S. Department of Energy
Office of Scientific and Technical Information
P.O. Box 62
Oak Ridge, TN 37831

Telephone: (865) 576-8401
Facsimile: (865) 576-5728
E-Mail: reports@adonis.osti.gov
Online ordering: http://www.osti.gov/bridge

Available to the public from
U.S. Department of Commerce
National Technical Information Service
5285 Port Royal Rd.
Springfield, VA 22161

Telephone: (800) 553-6847
Facsimile: (703) 605-6900
E-Mail: orders@ntis.fedworld.gov
Online order: http://www.ntis.gov/help/ordermethods.asp?loc=7-4-0#online

SAND2014-17329
Unlimited Release
September 2014

Thermal Characterization and Properties of a Copper-Diamond Composite

Pin Yang, Tom Chavez
Electronic, Optical and Nano-Materials (01816)

Christopher B. DiAntonio
FENG and Tube Lifecycle Engineering (02734)

Eric N. Coker
Advanced Materials Laboratory (01815)

Sandia National Laboratories
P.O. Box 5800
Albuquerque, New Mexico 87185-MS0958

Abstract

The thermal properties of a commercial copper-diamond composite were measured from below -50°C to above 200°C. The results of thermal expansion, heat capacity, and thermal diffusivity were reported. These data were used to calculate the thermal conductivity of the composite as a function of temperature in the thickness direction. These results are compared with estimated values based on a simple mixing rule and the temperature dependence of these physical properties is represented by curve fitting equations. These fitting equations can be used for thermal modeling of practical devices/systems at their operation temperatures. The results of the mixing rule showed a consistent correlation between the amount of copper and diamond in the composite, based on density, thermal expansion, and heat capacity measurements. However, there was a disparity between measured and estimated thermal diffusivity and thermal conductivity. These discrepancies can be caused by many intrinsic material issues such as lattice defects and impurities, but the dominant factor is attributed to the large uncertainty of the interfacial thermal conductance between diamond and copper.

ACKNOWLEDGMENTS

The authors would like thank Richard T. Knudson for his support and providing specially prepared copper-diamond composite samples for this study, Michael P. Saavedra for machining the composite with his excellent skills and expertise in wire electrical discharged machining (EDM) process, and Daniel K. Stefan for the final proof-reading of this report.

CONTENTS

FIGURES

TABLES

NOMENCLATURE

α	Temperature dependence of thermal diffusivity (or Alpha, cm^2/s)
C_p	Heat capacity under a constant pressure condition (J/(g*K) or J/(g*°C)
EDS	Energy dispersive spectroscopy
EMPA	Electron Microprobe Analysis
ρ	Density (g/cm^3)
λ	Thermal conductivity (W/(m*K) or (W/(m*°C)
L	Sample thickness, used in the thermal diffusivity measurement (mm or cm)
$\Delta L/L$	Thermal mechanical strain (or dL/L_o)
SEM	Scanning electron microscopy
$t_{1/2}$	Time required for back surface to reach half of the maximum temperature (s)
T_{max}	The maximum temperature that can be reached at the back of a thermal diffusivity sample (see Figure 2 for detail)
X-Y	In-plane direction
Z	Sample thickness direction

1. INTRODUCTION

The thermal properties of packaging materials play an important role for assuring device performance and system reliability. For example, heat dissipation is vital for high power and high density electronics because excess heat generated from active solid-state devices and resistors needs to be removed in order to assure the system performance and reliability. For these applications, a higher thermal conductivity for the packaging materials is essential. In other cases, thermal stresses generated by the localized heating from these electronic devices can ultimately cause solder, device or connection failures, and pose potential aging and reliability problems. Because thermal stresses are proportional to the modulus of material and the differences in thermal expansion coefficients, it is important to minimize the thermal expansion mismatch between active devices and packaging material so the risk of failures can be mitigated. Minimizing the thermal expansion mismatch is also vital to prevent thermal shock for electronic systems used in the extreme environmental conditions. Most of the time, optimizing the demands between thermal conductivity and thermal stresses are required to assure system reliability. Therefore, it is important to understand these thermal compatibility issues during the design phase to assure the performance and robustness of the electronic systems in their service conditions.

This report documents a few critical thermal properties of a commercial copper-diamond composite, including thermal expansion, heat capacity, thermal diffusivity and thermal conductivity. According to the information provided by our customer, this composite is consisted of a copper matrix and dispersed diamond particles. Copper has an excellent thermal conductivity (401 W/(m*K))[1] at room temperature, but it has a higher thermal expansion (16.5 -17.0 ppm/K). Carbon based materials, such as graphite, diamond-like carbon and diamond, have reported thermal conductivity ranging from a fair 80 W/(m*K) for graphite to greater than 2000 W/(m*K)) for diamond. Their linear thermal expansion coefficients span from 0.8 ppm/K for diamond to -1.5 ppm/K and to 8.378 ppm/K for graphite near room temperature in its in-plane and out-of plane directions, respectively.[2] Therefore, copper itself can serve as an excellent thermal spreader. When it is directly integrated with solid-state semi-conductor devices made of silicon or gallium arsenide or a low temperature co-fired ceramic module, the thermal stresses created by their thermal expansion mismatch during operation can be an issue. When combining copper and carbon based materials together as a composite, one can envision that the overall thermal conductivity will be reduced yet may still suffice to meet thermal dissipation demand in comparison to other plastic based package materials. In addition, the thermal expansion coefficient of these composites can also be reduced since linear thermal expansion coefficients of these carbon based materials are smaller. By exploiting the unique negative thermal expansion coefficient of graphite platelets in the in-plane direction through texturing technique (i.e., aligning platelets in a preferred orientation), the resulting composite can have a linear coefficient of thermal expansion closely matching to these semiconductor materials and low temperature co-fired ceramic modules.

In this study, we will measure the thermal expansion, heat capacity, and thermal diffusivity, and use these values to calculate its thermal conductivity in the -50 to 200 °C range. Other factors such as the impurity in the copper, particle size and physical properties of the carbon based

material(s), and overall microstructure and the degree of texturing, just to name a few, can also significantly impact these reported thermal properties. These will be omitted from the discussion as these factors were not characterized and investigated in this study due to time and budgetary constraints. These measured thermal properties will be compared and analyzed by a simple mixing rule. Curve fitting equations of these thermal properties based on the experimental data will be presented.

2. EXPERIMENTAL PROCEDURE

Two pieces of copper-diamond composite (12.85 mm(X) X 12.85 mm(Y) X 5 mm(Z), identified as TD-1 and TD-2) were provided for the thermal characterization. The first sample (TD-1) was machined into two discs (D = 12.70 mm) with 1.9 mm and 3.0 mm in thickness for the thermal diffusivity measurement. Because the constraint imposed by available sample size, it is unable to determine the thermal diffusivity in the in-plane direction (X-Y). The other sample (TD-2) was machined into bars of different geometries (12.85 mm X 5.10 mm X 5.10 mm, and 6.0 mm X 6.0 mm X 5.10 mm) for the thermal expansion measurement in the in-plane (X-Y) and thickness (Z) directions. The rest of the TD-2 sample was machined into two samples of 4.0 mm X 4.0 mm X 1 mm for the heat capacity measurement. These samples were machined by a wire-EDM (electrical discharge machining) technique, as the composite is difficult to machine by conventional methods.

2.1. Coefficient of Thermal Expansion

The thermomechanical response ($\Delta L/L$ versus temperature) of the copper-diamond composite in the in-plane and thickness directions was measured by a dilatometer equipped with a low temperature module (Netzsch, DIL 402C). The system was calibrated with a fused silica rod prior to the thermal expansion measurement. The thermomechanical response was recorded from -55°C to 280°C at 1°C/min. under flowing nitrogen. The instantaneous coefficient of thermal expansion (CTE) was determined by the first derivative of the thermal mechanical response with respect to temperature ($d(\Delta L/L)/dT$). A linear curve fitting by the least squares method of these instantaneous CTE data was employed to obtain the temperature dependence of CTE for density correction $\rho(T)$.

2.2. Heat Capacity

The heat capacity of the copper-diamond composite was measured from -140°C to 300°C at 6°C/min in a platinum pan under flowing helium (40 ml/min.) by a simultaneous thermal analyzer (Netzsch STA 409C/CD). The heat capacity was determined by a ratio method, using sapphire as a reference standard. Helium gas was used to enhance the heat transfer and to prevent water condensation during data collection. A third order polynomial equation was used for the curve fitting of these data. The curve fitting of the heat capacity data ($C_p(T)$) were later used to calculate the temperature dependence of thermal conductivity ($\lambda(T)$) of the copper-diamond composite.

2.3. Thermal Diffusivity

The thermal diffusivity was measured by a flash technique (Anter Flashline or TA EM-200). In this measurement, the temperature rise time on the rear side of the specimen generated by a short radiant energy pulse (High speed Xenon-pulse flash lamp, pulse with 400 to 600 μsec) on the front was recorded and analyzed by thermal transfer models. The system was equipped with a cold stage and data were collected between -75°C to 200°C in flowing argon. Argon was used to

avoid water condensation and to prevent oxidation of copper at higher temperatures. The thermal diffusivity can then be derived from the time ($t_{1/2}$) required for the back surface to reach half of the maximum temperature rise (1/2 T_{max}) displayed by the following relationship,

$$\alpha = 0.1388 \frac{L^2}{t_{1/2}} \qquad \text{(Eq. 1)},$$

where L is the specimen thickness.[3] Figure 1 illustrates the temporal response of temperature rise during a thermal diffusivity measurement. The input thermal pulse is illustrated by the red curve, while the change of temperature (detected by amplified thermocouple response (volts)) is given by the black curve. The immediate drooping behavior followed by the maximum temperature rise reflects the radiative heat loss from the sample surfaces to the surroundings. In this study, the radiative heat loss corrections are calculated based on Clark and Taylor's model. The temporal response was measured three times after the sample temperature reached its equilibrium condition. The average value of thermal diffusivity was calculated and reported for that temperature. Since the accuracy of the data depends on the agreement between the mathematical and experimental models, samples of two different thicknesses (L = 1.9 mm and 3.0 mm) were used to verify our measurements. To interpolate the temperature dependence of thermal diffusivity (α(T)) between data points a curve fitting of the final data was given by a second order polynomial equation.

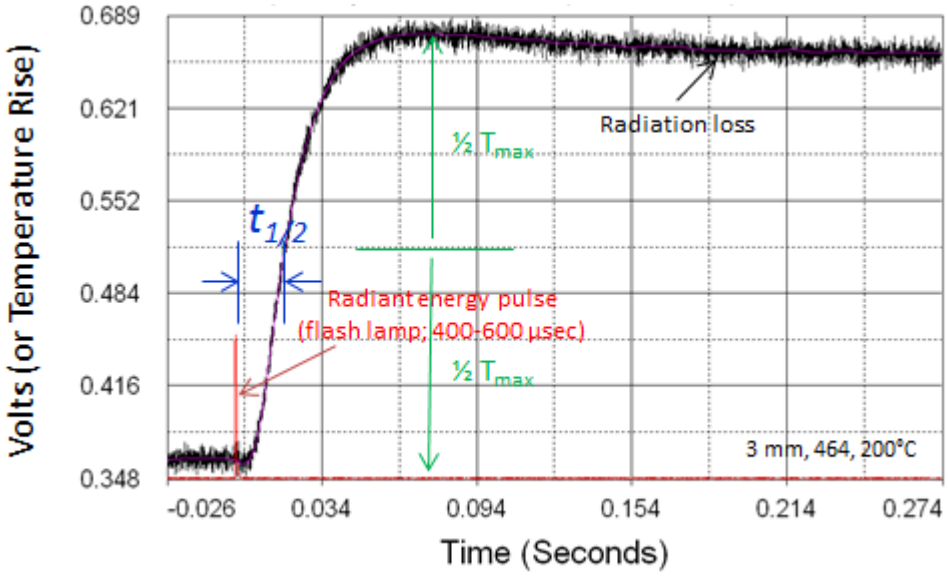

Figure 1. The temporal response for temperature rise time at the back of the sample after radiant energy pulse is released (taken from 3 mm thick copper-diamond sample at 200°C).

Since we have extensive experience in heat capacity and thermal mechanical measurements, these data were collected based on our standard correction and collaboration procedures. However, we lack practical experience in the thermal diffusivity measurement with the current system at subambient conditions. Therefore, in this report we used two NIST samples, including a thermographite and an electrolytic iron, to benchmark our measurements [Appendix A and Appendix B], and three oxygen-free copper disks (L = 2 mm, 3 mm and 3.5 mm) to compare the

temperature dependence of thermal diffusivity and thermal conductivity against the literature data [Appendix C and Appendix D]. These experiments would cover a wide thermal diffusivity range (0.2 to 1.2 cm^2/s), and should give us basic information about system precision and accuracy. The data collected from thermographite and oxygen-free copper can also be used for graphite and copper to estimate the thermal diffusivity and thermal conductivity of the studied composite material.

2.4. Thermal Conductivity

The temperature dependence of thermal conductivity ($\lambda(T)$) of the copper-diamond composite was directly calculated from the curve fitting values of thermal diffusivity, density, and heat capacity displayed by the following relationship

$$\lambda (T) = \alpha (T)\, \rho(T)\, C_p(T) \qquad \text{(Eq.2).}$$

3. RESULTS AND DISCUSSION

3.1. Density

The bulk density of as-received samples was measured by the Archimedes method at room temperature. Note these specially fabricated samples do not have any electroplated materials on the surfaces. The measured bulk density for specimens TD-1 and TD-2 were 5.547 g/cm^3 and 5.451 g/cm^3, respectively. The average density of the composite is 5.499 g/cm^3 which is close to the bulk density of similar commercial products [Appendix F, Cu MetGraf 4-280]. If we assume the density values of diamond and graphite are 3.51 g/cm^3 and 2.25 g/cm^3,[1] this corresponds to a 63.5 vol.% of diamond or a 51.6 vol.% of graphite in the composite structure. These values immediately suggest that this composite is heavy loaded with a second phase or filler (diamond or graphite). As it can be seen later from the thermal expansion, heat capacity measurements and mixing rule calculations, the filler in this composite is most likely to be diamond. However, we have no other evidence to support this assumption. Based on these reasons, the term "copper-diamond composite" is used to represent the material under this investigation.

3.2. Thermal Expansion

The thermomechanical response ($\Delta L/L$ vs. T) for the copper-diamond composite in the in-plane (X and Y) and the thickness (Z) directions is given in Figure 2 to Figure 4. Figure 2 and Figure 3 each show two consecutive measurements on heating (red) and cooling (blue) cycles in the X and the Y directions, respectively. The two curves on each figure are almost overlapped suggesting these measurements are quite reproducible and consistent. In both cases, the thermally induced strain shows slightly nonlinear increase with temperature (concave curves), which simply mirrors the temperature dependence of the bond relaxation due to the anharmonicity of the interatomic potential in the copper or the diamond lattice. A similar measurement is performed in the thickness (Z) direction. Based on these data sets, the technical CTEs in the X, Y and Z directions at two different temperature ranges are summarized in Table 1.

Table 1. Technical thermal expansion coefficients for the copper-diamond composite.

Direction of measurement	Technical coefficient of thermal expansion (ppm/°C, or ppm/K)	
	In -40°C to 125°C range	In 125°C to 270°C
X (In-plane)	6.8460	8.9152
Y (in-plane)	6.0817	7.6704
Z (Thickness)	6.2486	8.1950

These data indicate that there is a noticeable anisotropy in the in-plane (X-Y) where the CTE values in the X direction are slightly higher than the Y direction at these temperature ranges. These CTE values are better matched with the thermal expansion of silicon (2.6-10 ppm/°C), gallium arsenide (5.39 ppm/°C), and low temperature co-fired ceramic (~7 ppm/°C). Therefore, this composite can minimize the thermal stresses if it is used with these materials for advanced packaging applications. However, these values are higher than the in-plane CTE value reported (i.e., 4 ppm/°C) in the product specification sheet.[Appendix H, assume Cu MetGraf 4-280].

The instantaneous coefficient of thermal expansion at different temperatures (d(ΔL/L)/dT, dotted line) was calculated from the slopes of these thermomechanical responses. These instantaneous CTEs in different directions are plotted in Figure 5 and are fitted with a linear equation by a least squares method. The results indicate that the composite material exhibits a linear increase in its thermal expansion coefficient in this temperature range, suggesting the anharmonic term of the interatomic potential is a linear function of temperature – a common observation and practice used for first-order approximation in materials modeling. Results show the temperature dependence of CTE(T) (unit: 1/°C) can be expressed as

X direction $\quad CTE(T, °C) = 1.3887E\text{-}8*T+6.2641E\text{-}6 \ (R^2 = 0.993)$ (Eq.3)

Y direction $\quad CTE(T, °C) = 1.1608E\text{-}8*T+5.5960E\text{-}6 \ (R^2 = 0.993)$ (Eq.4)

Z direction $\quad CTE(T, °C) = 1.2264E\text{-}8*T+5.7148E\text{-}6 \ (R^2 = 0.993)$ (Eq.5)

The estimated CTE(25°C) at room temperature ranges from 6.61 ppm in the X direction and between 6.00 to 6.02 in the Y and Z directions. The thermal expansion coefficients at room temperature for graphite in the in-plane direction and the Z direction are -1.5 ppm/°C and 8.378 ppm/°C.[2] The unusual negative CTE is due to transverse vibrations of carbon in the planar direction.[4] The CTEs for diamond, polycrystalline carbon and copper are 1 ppm/°C, 7.1 ppm/°C and 16.5 ppm/°C. Based on these data, the mixing rule will immediately exclude the possibility of using polycrystalline carbon as the second phase in the composite since the calculated solid loading of the polycrystalline carbon will be greater than 100%. Second, if the composite consisted of highly textured graphite, the amount of preferentially aligned planar graphite should occupy about 70.2 vol. % in the X direction in order to take advantage of the negative CTE in the X direction. The estimation is too high, if not practically impossible. In addition, if the composite is indeed a textured copper-graphite composite, the thermal expansion coefficient should be strongly anistropic as illustrated by the values in the Appendix F. Lastly, if we consider diamond is the disperse second phase and use the average CTE value for the composite at room temperature, this mounts to 63.8 vol.% of diamond in the composite, which is very close to the density estimation (i.e., 63.5 vol.%). From a processing viewpoint, this solid loading is achievable.

Based on these CTE values, the change of density as a function of temperature for this composite is calculated from the linear curve fitting equations from Eq.3 to Eq.5, and the results of density versus temperature ρ(T) (unit g/cm^3) is plotted on Fig. 5 and given in Equation 6.

$$\rho(T, °C) = 5.4990 - 2.0765E\text{-}7*T \qquad \text{(Eq.6)}$$

The temperature dependence of density, ρ(T), will be used to calculate the thermal conductivity based on Equation 2.

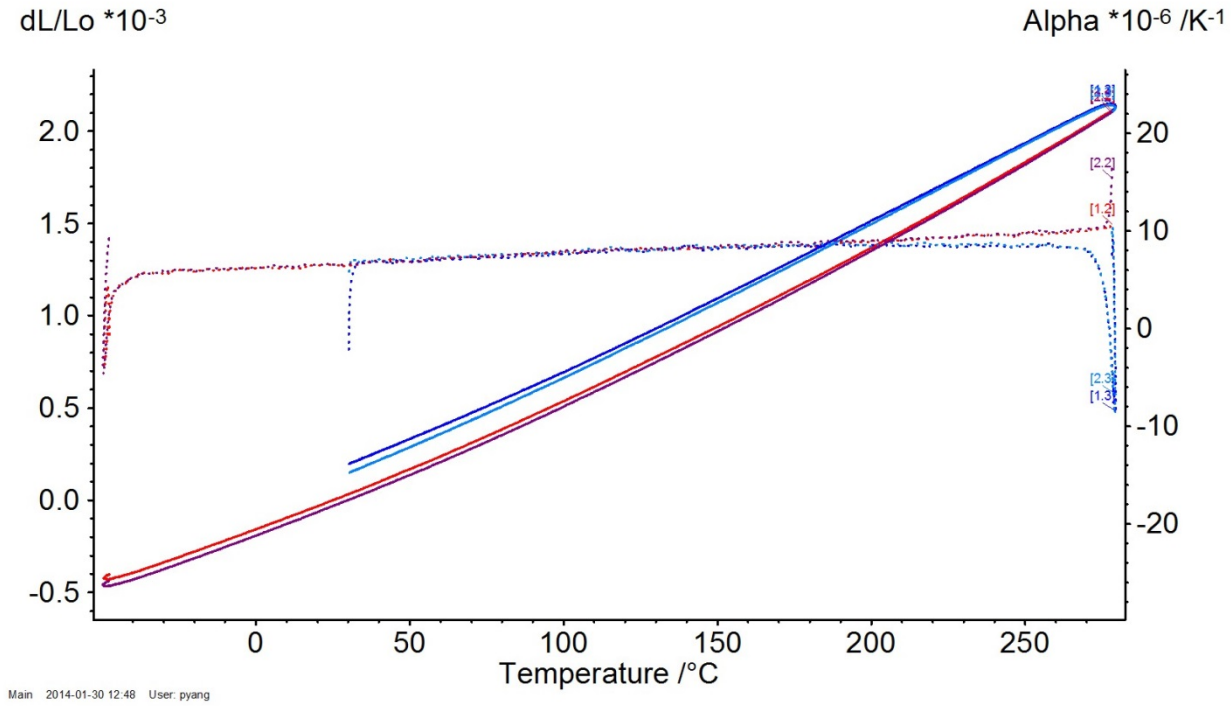

Figure 2. The thermomechanical response and the instantanous coefficient of thermal expansion (dotted line) for the copper-diamond composite in the in-plane X direction collected from two measurements, (red curves are on heating and blue curves are on cooling).

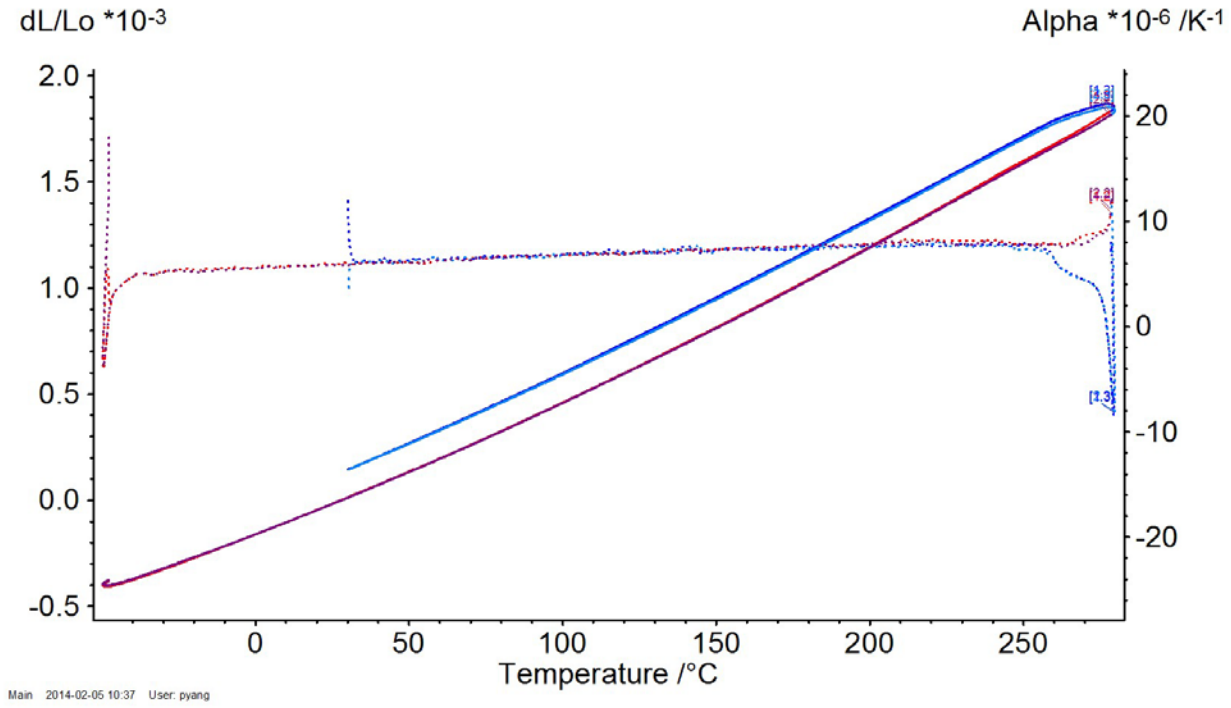

Figure 3. The thermomechanical response and the instantanous coefficient of thermal expansion (dotted lines) for the copper-diamond composite in the in-plane Y direction collected from two measurements, (red curves are on heating and blue curves are on cooling).

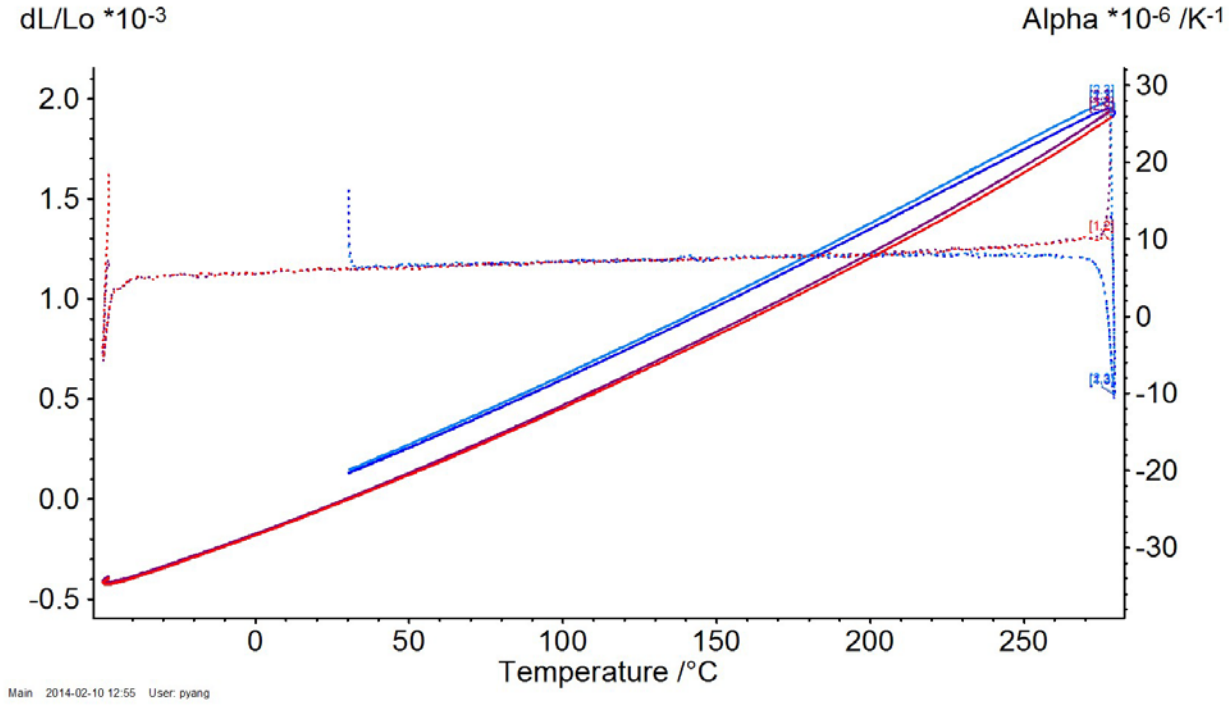

Figure 4. The thermomechanical response and the instantaneous coefficient of thermal expansion (dotted lines) for the copper-diamond composite in the thickness (Z) direction.

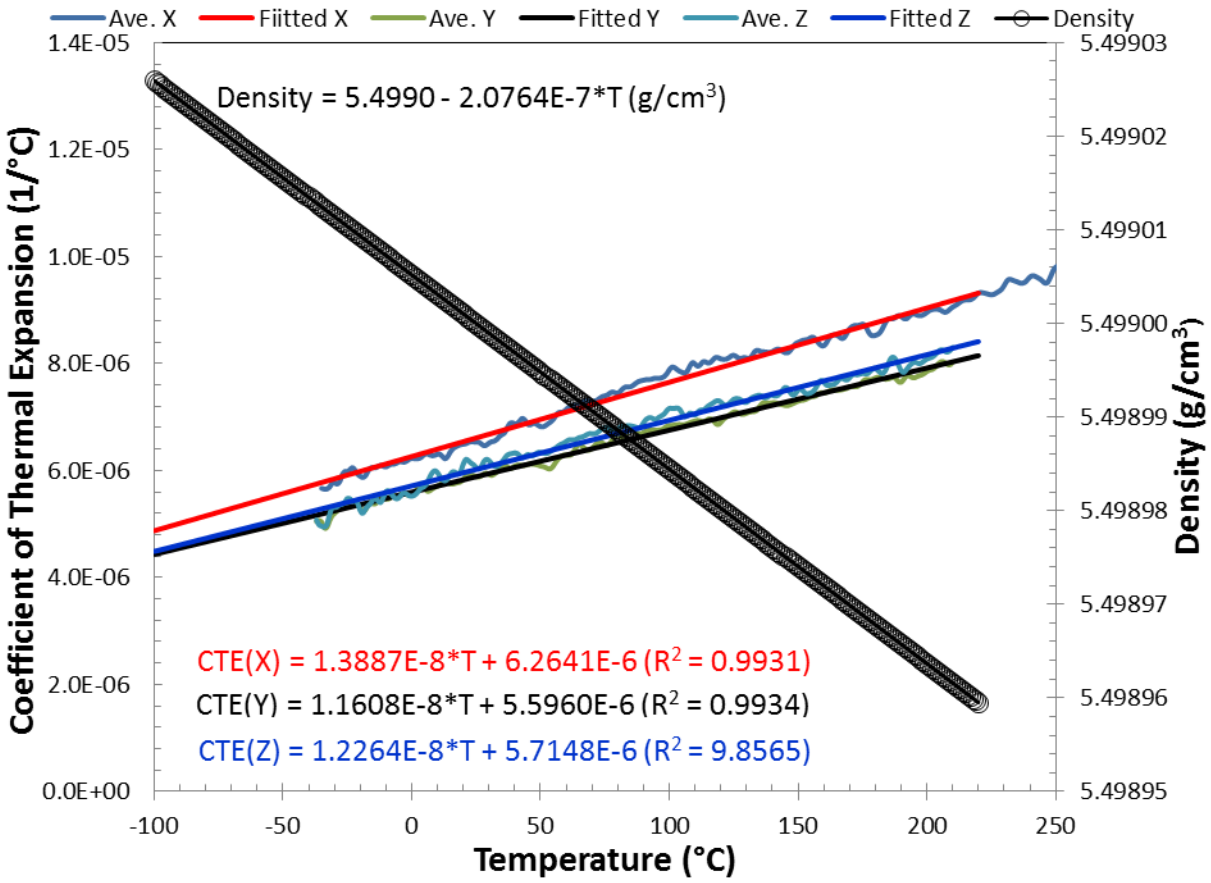

Figure 5. The coefficient of thermal expansion and density (black open circle) as a function of temperature in the in plane direction for the copper-"diamond" composite.

3.3. Heat Capacity

The heat capacity for the copper-diamond composite was measured from -140°C to 300°C at 6°C/min. The experiment was repeated three times and the results were very consistent. One set of these measured data (illustrated by the blue line) is plotted against temperature in Figure 6. The small oscillation observed in the data set is caused by the temperature fluctuations from the air condition in the laboratory. The heat capacity data were fitted with a third order polynomial (red curve) with respect to temperature, and the temperature dependence of $C_p(T)$ (unit: J/(g*°C)) in this temperature range can be expressed as,

$$C_p(T, °C) = -3.8056E\text{-}9*T^3 + 2.9866E\text{-}7*T^2 + 1.4488E\text{-}3*T + 3.9471E\text{-}1 \quad (R^2 = 0.999) \qquad \text{(Eq.7)}$$

The use of a third order power fitting routine is based on the Debye approximation for heat capacity. The calculated heat capacity for this composite at room temperature is 0.4389 J/(g*°C). Based on a simple mixing rule and heat capacity values of 0.385 J/(g*°C) and 0.7 J/(g*°C) for copper and graphite, the estimated weight percent of graphite in the composite is about 17.1 wt.%, which corresponds to 45.1 vol.%. This value is slightly lower than the density estimation (50.1%). Once again, if we use diamond (Cp = 0.5091 J/(g*°C) instead of graphite, the mixing

rule gives a 43.43 wt.% of diamond. Using the specific density of copper (8.96 g/cm^3) and diamond (3.51 g/cm^3), this leads to a 66.2 vol% of diamond, which is in a good agreement with the values estimated from density (63.5 vol.%) and CTE (63.8 vol.%) calculations.

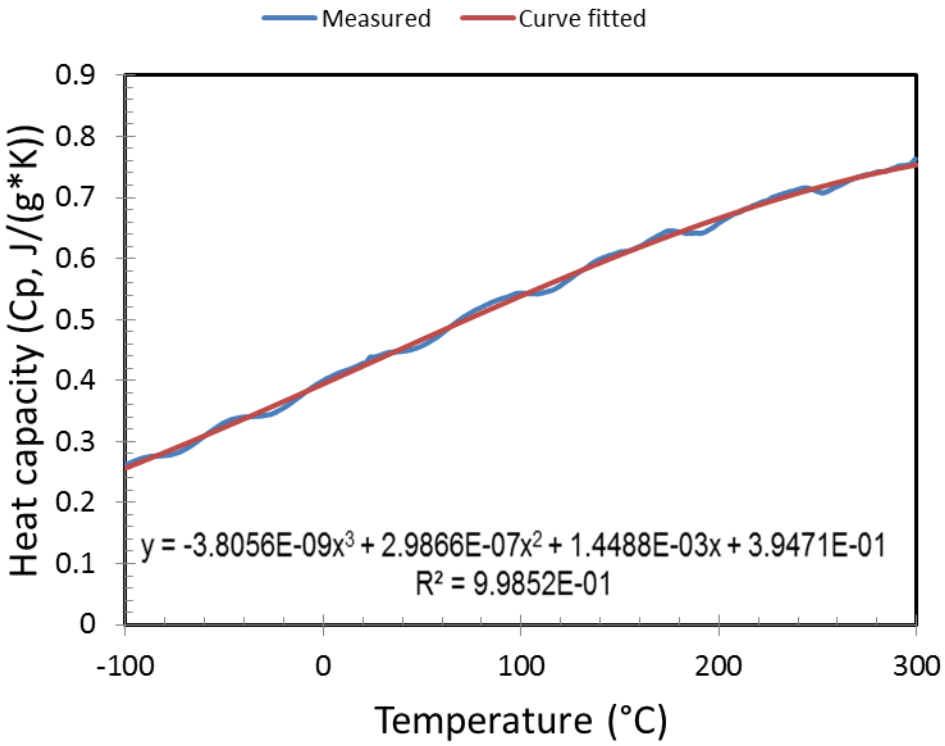

Figure 6. The temperature dependence of heat capacity for the copper-diamond composite. The blue and red curves represent the measured and curve fitting data, respectively.

3.4. Thermal Diffusivity

The thermal diffusivity is measured in the thickness direction (Z) from samples of two different thicknesses (L = 1.9 mm and 3.0 mm). Figure 7 shows the measured thermal diffusivity verse temperature from a 1.9 mm thick sample based on two independent measurements (blue diamonds (run# 469) and red squares (run# 471)). These data are collected from two back-to-back measurements set at 5°C apart between each run without re-arranging the sample in the sample holder. A curve fitting for this data was implemented, and the calculated thermal diffusivity based on the fitting results was given by the green line between -100°C to 220°C. Results show that these measurements are consistent and all the data is within the 4% error range. Figure 8 gives the same measurement results from a 3.0 mm thick sample collected from three different runs blue diamond (run# 464), red square (run# 465), and purple triangle (run# 466). The test run # 464 is the first run and the results are greater than the 1.9 mm sample. This caused some concerns and the sample was taken out and inspected, then placed back to the sample holder and measured again. Two consecutive back-to-back runs (runs #465 and #466) were performed without rearranging sample in the holder. These two runs exhibit an excellent consistency (red squares and purple triangles). However, these data varies significantly from the first run (run #464), particular at the low temperature range (~15%), but the difference becomes

smaller as the temperature approaches 200°C. Because these disc samples are slightly smaller than the fixture hole, it is speculated that heat losses from the edge of these disks might contribute to these discrepancies, particularly if the edge is in contact with the sample holder This is supported by the excellent reproducibility of #469 and #471 runs for the 1.9 mm sample and #465 and #366 runs for the 3 mm sample, where the heat losses between each back-to-back measurement should be almost identical, as each sample is fixed in the same configuration in the fixture. If the same sample is under a different configuration, for example, the edge of the disc does not come in contact with the fixture (or has less contact area) this will lead to a faster rise time as thermal pulse can propagate through the thickness direction without losing a significant amount of the heat from the edge to the surroundings. This edge effect can influence the accuracy of the thermal diffusivity measurement, particular for materials of high thermal conductivity. Less contact with the surroundings (or fixture) reduces the amount of heat loss and results in a higher thermal diffusivity (as seen for first run, #464). This edge effect manifests itself when comparing thermal diffusivity values for samples of different thicknesses. Based on the same argument, a thinner sample will have less heat loss from its edge; therefore, it is anticipated that the measured thermal diffusivity should be higher. This is illustrated in Figure 9 (red squares are for 3.0 mm sample and blue diamonds are for 1.9 mm sample) where the thermal diffusivity of 1.9 mm sample is higher than 3.0 mm sample at lower temperatures and the difference diminishes as temperature rises. The decreases in the difference at higher temperatures can be attributed to the increase of thermal resistivity due to electron/phonon scattering in the lattice (both copper and the dispersed diamond) and the radiation loss becomes more dominant than conduction losses. This makes the thermal losses from the edge a minor effect. Therefore, the observed discrepancies can be attributed to thermal losses due to the change of sample configuration in the sample holder. Additional evidence that supports the heat loss argument (an artifact) for the 3.0 mm sample between shot #464 and #466 near room temperature is given in Appendix E. Based on these observations, it is sensible to use the highest thermal diffusivity data for the copper-graphite composite. In this study, the highest thermal diffusivity from all these measurements (#464) will be used for thermal conductivity calculation. Based on the curve fitting results, the average thermal diffusivity (unit: cm^2/s, the green line on Figure 10) of this composite can be described as

$$\alpha(T, °C) = 5.9673E\text{-}6*T^2\text{-}3.2553E\text{-}3*T+1.0110 \ (R^2 = 9.9894) \qquad \text{(Eq.8)}.$$

When comparing the thermal diffusivity of this composite at room temperature (°C), the thermal diffusivities from the fitting for 1.9 mm, 3.0 mm are 0.849 to 0.933 cm^2/s. These values are significantly lower than copper and diamond which are 1.22 cm^2/s and 3-11 cm^2/s. [Appendix C, Figure 15], but higher than graphite which is 0.54 cm^2/s [Appendix A, Figure 13].

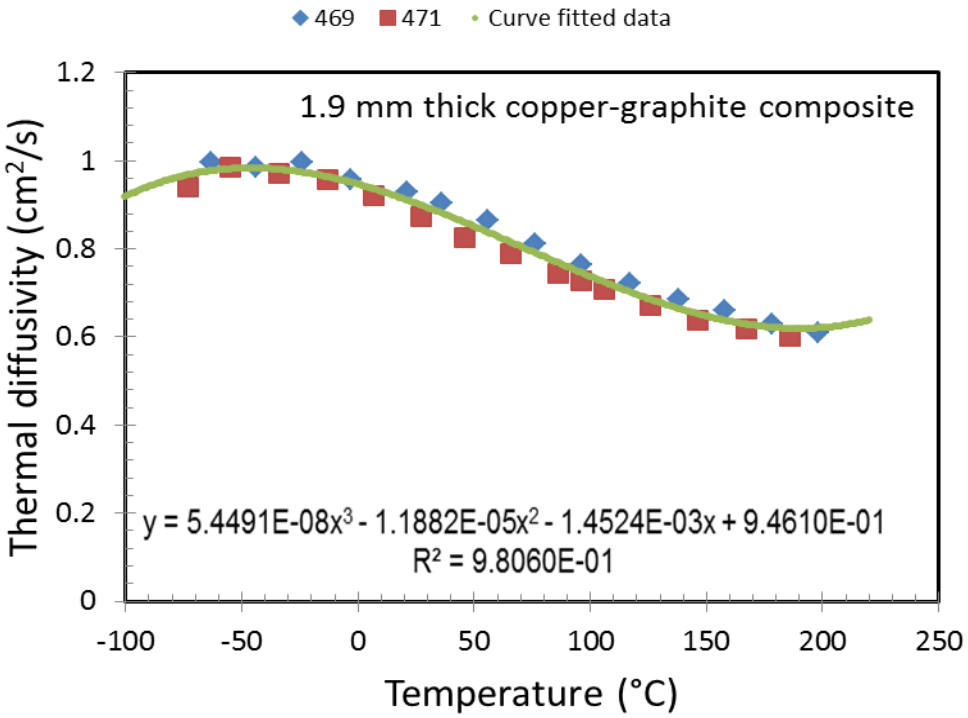

Figure 7. The measured thermal diffusivity values for a 1.9 mm thick copper-diamond composite. The average fitting data are represented by the green line.

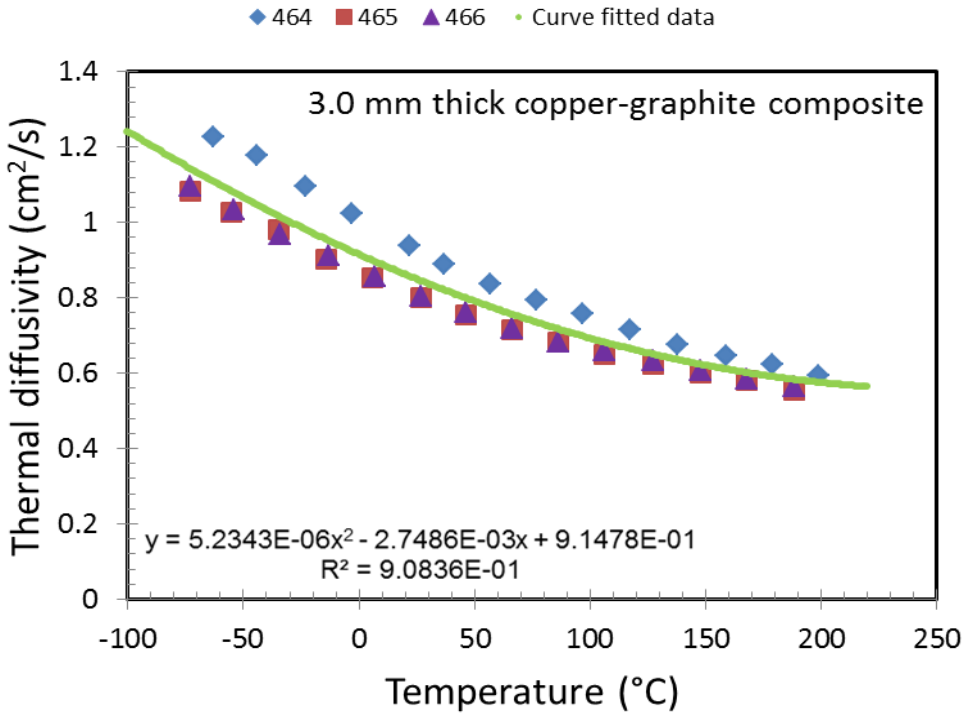

Figure 8. The measured thermal diffusivity values for a 3.0 mm thick copper-diamond composite. The average fitting data are represented by the green line.

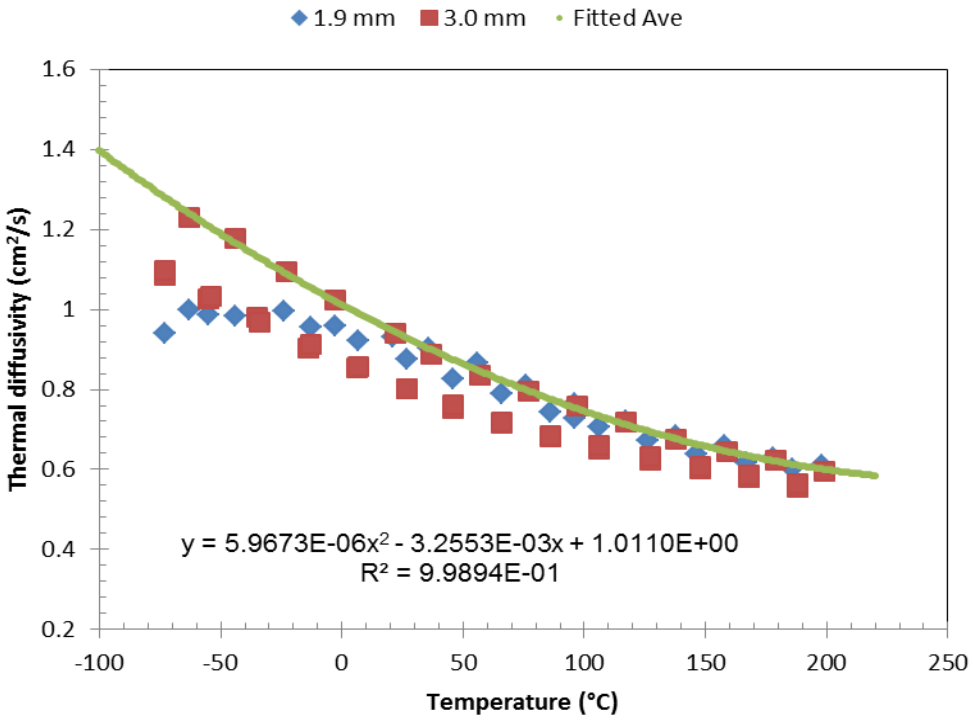

Figure 9. The measured thermal diffusivity values for a 1.9 mm and a 3.0 mm thick copper-diamond composite samples. The average fitting result for the highest thermal diffusivity measurement from the 3 mm thick sample are represented by the green line.

3.5. Thermal Conductivity

Based on the curve fitting results from density (Eq. 6), heat capacity (Eq.7, red) and thermal diffusivity (Eq. 8, blue), the temperature dependence of thermal conductivity (λ(T), W/(m*K), black) is calculated based on equation (2) and the results are given in Figure 10. Several experimental data (circles) are selected and added to the figure for comparison purposes. The curves results suggest that the thermal conductivity of this composite can be depicted by a third-order equation as given in Equation (8),

$$\lambda(T, °C) = 220.70 + 1.1767E\text{-}1*T\text{-}1.3128E\text{-}3*T^2+3.8368E\text{-}6*T^3 \ (R^2=0.9997) \qquad \text{(Eq.8).}$$

Based on this relationship, the calculated thermal conductivity at room temperature is 223 W/(m*K). This value, at the first glance, is better than polycrystalline graphite (~80 W/(m*K)), but much lower than copper (~ 400 W/(m*K)) and far below the value of diamond (600 to 2000 W/(m*K)). However, heat conduction in a composite with a dispersed second phase is usually limited by the poorer conductor phase since the thermal conductivity of this type composite is best estimated by a parallel conduction model. In this case the limiting conductor in the composite is copper. As a result, the estimated lower bound for the thermal conductivity should be greater than or equal to 400 W/(m*K), which is much higher than the measured value. This discrepancy immediately suggests additional mechanisms must be involved in the heat transfer

process and the thermal conductivity calculation. These mechanisms should further reduce the thermal mean-free-path and lead to a lower thermal conductivity. Several mechanisms may contribute to this behavior including (1) impurities in copper and/or in diamond, as impurities can effectively reduce the thermal conductivity in materials, (2) additional thermal scattering by the dispersed second phase, since the second phase like impurity can enhance phonon scattering and result in a lower thermal conductivity, and (3) thermal conduction loss at the copper-diamond interface, this could be a result of a weakly bounded interface where conduction cannot efficiently transfer from one phase to the other, or due to the inefficiency of heat transfer from electronic dominated heat conduction in copper to the phonon dominated heat conduction in diamond, just to name a few. The last mechanism is supported by how easy these dispersed diamonds can be rubbed off from the surfaces of these EDM specimens. The weak interface and the aforementioned scattering mechanisms will further reduce the average phonon mean-free-path for heat conduction, resulting in a thermal conductivity lower than the lower bound of copper.

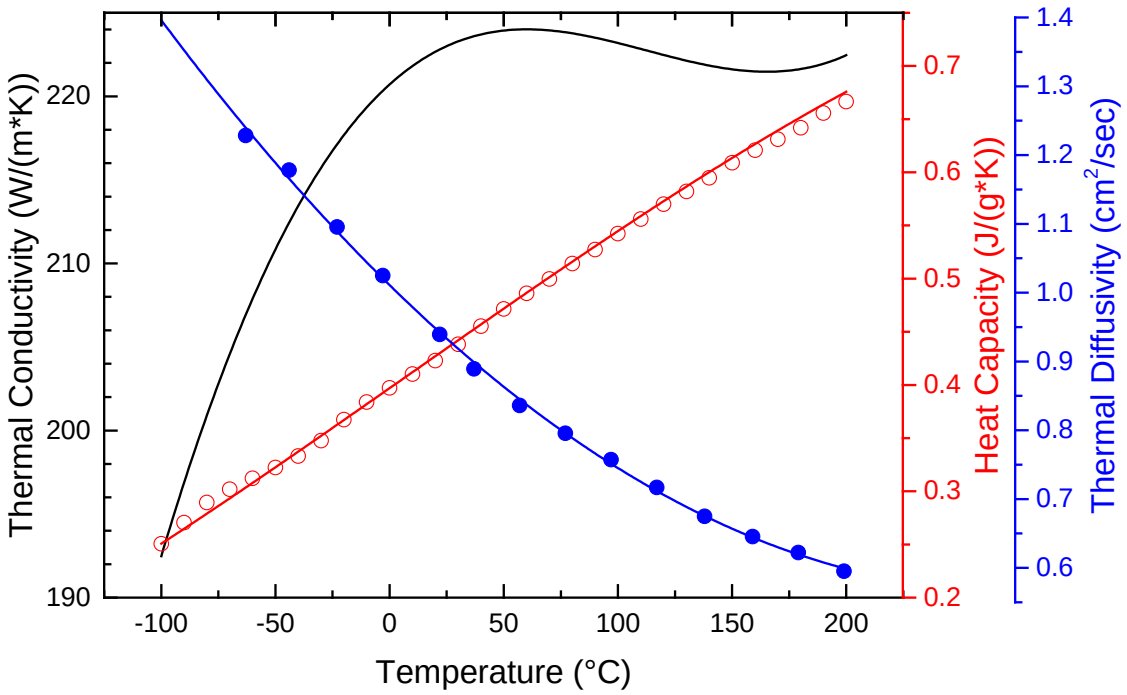

Figure 10. The summary of all the thermal properties of a copper-diamond composite in the -100 to 200°C range.

Literature has predicted high thermal conductivity values for these copper-diamond composites. [5] An example of such a prediction is given in Figure 11.[5] This effective thermal conductivity of the composite on this figure is based on thermal resistors in series, where its value depends on the thermal conductivity of the matrix and the dispersed phase, as well as the size of the dispersions and the interfacial conductance. When the interfacial conductance is fixed (0.7 W/(cm^2*K)) as illustrated in this figure, it is clear that the effective thermal conductivity increases with the diamond loading and its particle size. However, this model fails to show the impacts of percolation (when diamond and diamond particles are in contact)[6] on thermal

conductivity of the composite, when the volume fraction of diamonds exceeds ~67 vol.%. It is anticipated under that condition, the thermal conductivity will increase dramatically.[6] Based on this model, when a composite is loaded with a 60 volume percent of 100 μm diamond particles, as it resembles the composite we studied in this work, the estimated thermal conductivity should be close to 650 W(/m*K), which is much greater than 223 W/(m*K) that was derived from our experimental results. In comparison, a thermal conductivity value between 445 and 480 W/m*K has been measured and reported for a similar hot-pressed copper-diamond composite (50 vol. % diamond). [7] However, the experimental details, measurement errors, and interface modification were not clearly documented in that publication. These calculated and measured values are all greater than our experimental data. Therefore, it is believed this large discrepancy could be attributed to the uncertainty in the interfacial conductance between diamond and copper which is illustrated in Figure 12.[5] As it is illustrated in this figure, when interfacial conductance is high (0.1 to 0.01W/(m^2*K)), the calculated effective thermal conductivity converges near 800 W/(m*K), regardless of the particle size of the diamond. As the interfacial conductance decreases below10^{-6} W/(m^2*K) and becomes the major contributor to the overall thermal impedance of the composite, the effective thermal conductivity will be lower than the copper matrix (as shown by the curves on the left bottom corner). Based on this model and our experimental results, the estimated interfacial conductance for our composite is just below 10^{-6} W/(m^2*K). In fact, even with an interface engineering, some authors have concluded that it is almost impossible to achieve an effective thermal conductivity greater than a value higher than that of copper.[8] These observations highlight the importance of interfacial conductance on the effective thermal conductivity of a high diamond loading copper composite.

In addition to the thermal conduction loss at the copper-diamond interface, the calculated curve in Figure 10 suggests that the thermal conductivity of this composite is dominated by the high volume loading of diamond. Since in this temperature range the thermal conductivity of copper decreases and levels off to its minimum value (-173°C) long before temperature increases to room temperature, the observed increasing of thermal conductivity from -100°C to 200°C must be attributed to the high diamond loading (or phonon conduction) in the composite.

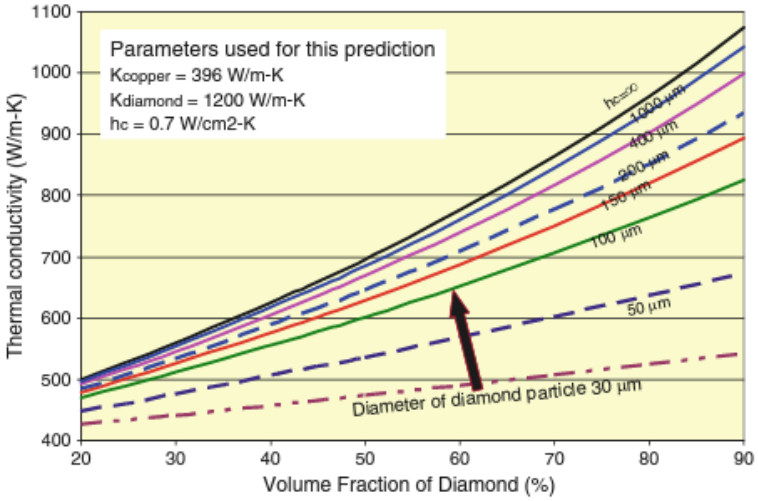

Figure 11. Illustration of thermal conductivity with various volume fraction and particle size of diamond in a copper matrix.[5]

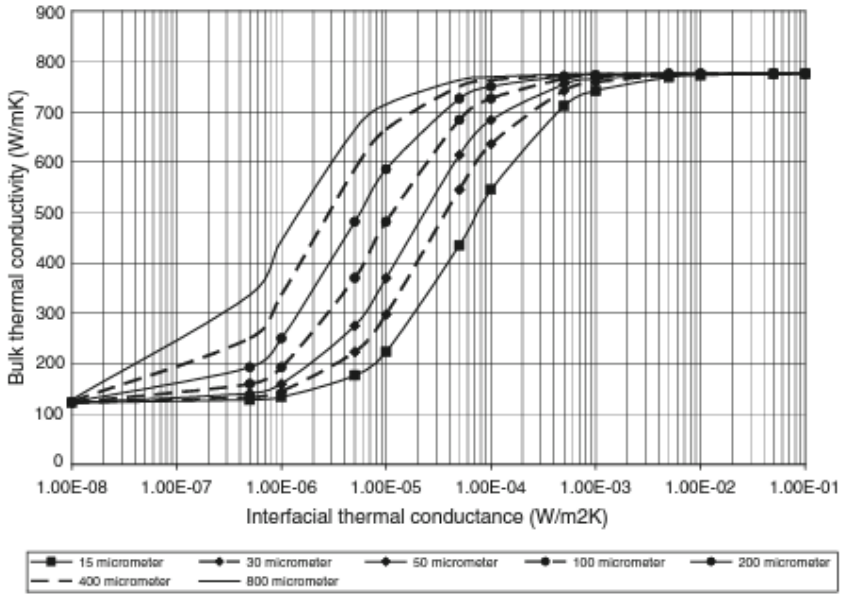

Figure 12. Illustration of the effective thermal conductivity variation with interfacial conductance for 60 percent volume of diamond-copper composites (with different sizes of dispersed diamond).[5]

4. SUMMARY

In this brief study, we have experimentally measured the thermal expansion, heat capacity and thermal diffusivity of a copper-diamond composite as a function of temperature from -50°C to 200°C. These data were used to calculate the thermal conductivity parallel to the sample thickness direction. Density measurements indicate this composite has a high volume loading (> 60 vol.%) of the dispersed phase. The coefficient of thermal expansion in the in-plane direction from -40°C to 125°C (7.7 to 8.9 ppm/°C) is closely matched with the thermal expansion of low temperature co-fired ceramic and gallium arsenide. The heat capacity of this composite near room temperature is 0.44 J/(g*°C). Within the temperature range of this study, the thermal conductivity of the composite increases with temperature and levels off near 50°C. The thermal conductivity (223 W/(m*K)) determined from the experimental data is lower than thermal conductivity of the copper matrix (~ 400 W/(m*K). The decrease in the thermal conductivity is attributed to the low interfacial conductance between copper and diamond. Therefore, incorporation of diamond particles into a copper matrix can effectively reduce its coefficient of thermal expansion coefficient but may not be able to enhance the thermal conductivity of the composite, unless the interfacial conductance issue is resolved. In the future, it will be beneficial to add detailed characterization for the diamond (by X-ray or Raman) used in the composite, and quantitative chemical analysis at the copper-diamond interface (by EMPA or EDS), as well as the overall microstructure of the composite (SEM). The information will help us better understand the issues and properties of this composite material.

5. REFERENCES

1. R. C. Weast and M. J. Astle, *CRC Handbook of Chemistry and Physics*., 63rd edition, CRC Press, Inc. Boca Raton, Florida, (1984).
2. J. B. Nelson and D. P. Riley, "The Thermal Expansion of Graphite from 15°C to 800°C: Part I; Experimental)," *Physical Soc*., **50** [6] 447-486 (1945).
3. W. J. Parker, R. J. Jenkins, C. P. Butler, and G. L. Abbott, "Flash Method of Determining Thermal Diffusivity, Heat Capacity, and Thermal Conductivity," *J. Appl. Phys*., **32** [9] 1679-1684 (1961).
4. A. C. Bailey and B. Yates, "Anisotropic Thermal Expansion of Pyrolytic Graphite at Low Temperatures,' *J. Appl. Phys*., **41** [13] 5088-5091 (1970).
5. Xingcun Colin Tong, *Advanced Materials for Thermal Management of Electronic Packaging*, Springer Series in Advanced Microelectronics, Vol. 30. Springer (2001).
6. Y-M Chiang, D Birnie III, and W. D. Kingery, *Physical Ceramics – Principles for Ceramic Science and Engineering*,"MIT series in Material Science and Engineering Vol. 1, Chapter 5, p. 474-477 Wiley (1996)
7. J. Barcena, J. Maudes, M. Vellvehi, X. Jorda, I. Obieta, C. Guraya, L. Bilbao, C. Jimenez, C. Merveille, and J. Coleto, "Innovative Packaging Solution for Power and Thermal Management of Wide-bandgap Semiconductor Devices in Space Applications, *Acta Astronautica*, 62, 422-430 (2008).
8. J. Barcena, M. Garica de Cortazar, R. Seddon, J. C. Lyoyd, A. Torregaray, and J. Coleto, "Effect of the Incorporation of Interfacial Elements on the Thermophysical Properties of Cu/VGCNFs Composites," Composites Science and Technology, 70, 2258-2262 (2010).

6. APPENDIX

A. Thermal Diffusivity of Thermographite

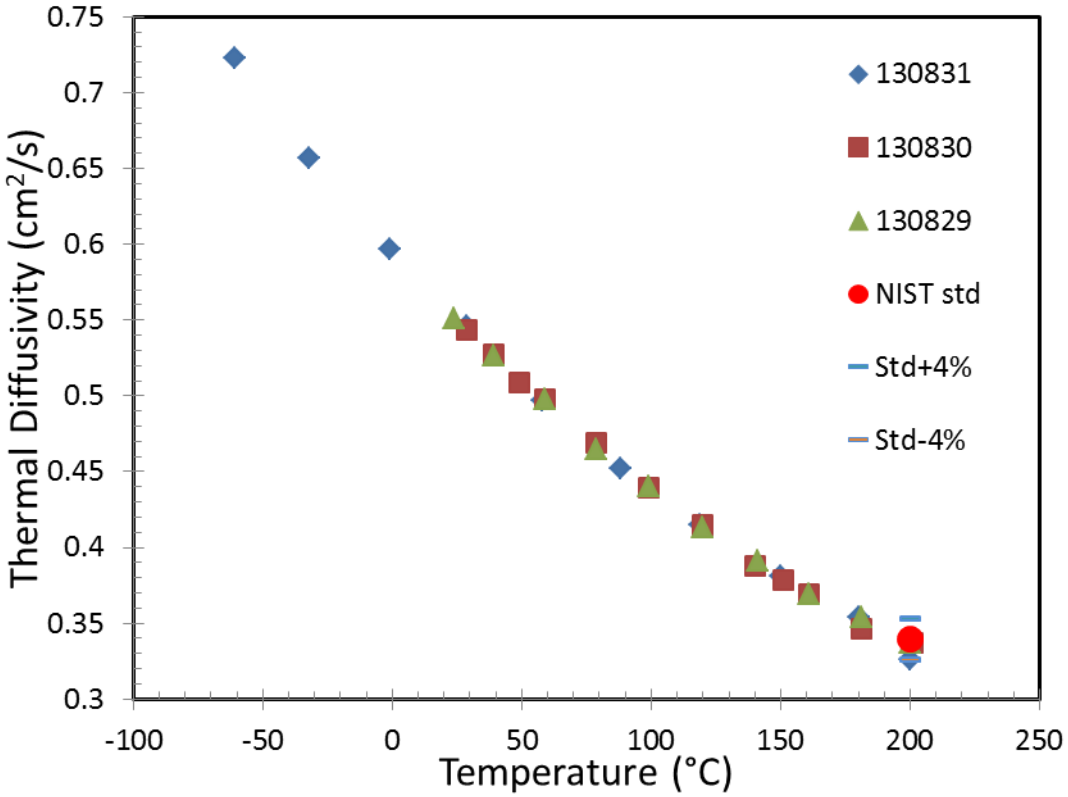

Figure 13. The measured thermal diffusivity for thermographite from -70°C to 200°C. A NIST data point (Red dot) at 200°Cwith 4% standard deviation is added for comparison purposes.

Figure 13 collects thermal diffusivity data of the thermographite from three different runs (including 130829,130830, 130831). The red dot overlaid on the figure is a single datum reported from NIST thermal diffusivity data sheet at 200°C (with ±4% makers). The NIST data sheet does not include any data below 200°C since this sample is usually used as a calibration standard for high temperature measurements (>1000°C). The results exhibit a monotonic decrease in thermal diffusivity with increasing temperature and match the NIST data well at 200°C, suggesting the errors of our measurement is within 4%.

B. Thermal Diffusivity of Electrolytic Iron

Figure 14 shows the change of thermal diffusivity of electrolytic ion as a function of temperature from -70°C to 200°C. Data were collected from three different measurements (130829, 130830, 130831). These data are overlaid and these red dots are data taken from NIST data sheet. Results indicate that errors of the thermal diffusivity measured by our test system should be below 4%, both thermographite (Fig. 13) and electrolytic ion (Fig. 14).

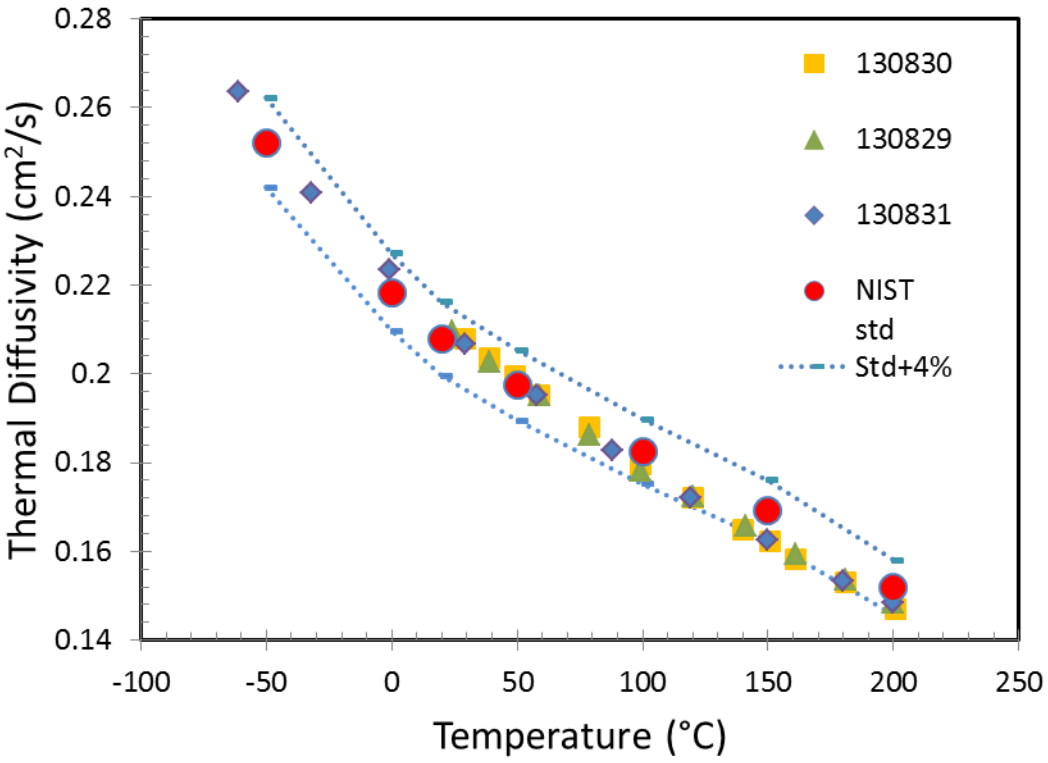

Figure 14. The measured thermal diffusivity of electrolytic iron from -70°C to 200°C. The red dots are literature data from NIST data sheet and the dotted blue lines are boundaries of ±4% for each data point.

C. Thermal Diffusivity of oxygen-Free Copper

The thermal diffusivity of oxygen-free copper was independently measured with three different sample thicknesses (i.e., L = 2mm, 3 mm, and 3.5 mm). Since copper possesses high thermal diffusivity, materials of this kind, particular with a thinner geometry, will produce a rapid temperature raise curve when compared to the temporal response of the input radiant thermal pulse (see Fig. 1 - red curve), making mathematical and fitting calculation extremely challenge. This can lead to large errors in the thermal diffusivity and the phenomenon is commonly known as the "finite pulse width effect." From Figure 15, it is obvious that the data collected from the thinnest copper disc (i.e., 2 mm disc, blue legend) shows a large variation and is greatly deviated from the rest of the data sets, indicating that the thermal diffusivity measurements might suffer from the "finite pulse width effect." Data measured by the 3 mm and the 4 mm thick discs are reasonably consistent except in the 60-75°C range. These data slightly higher than the data reported in the literature (yellow dot).

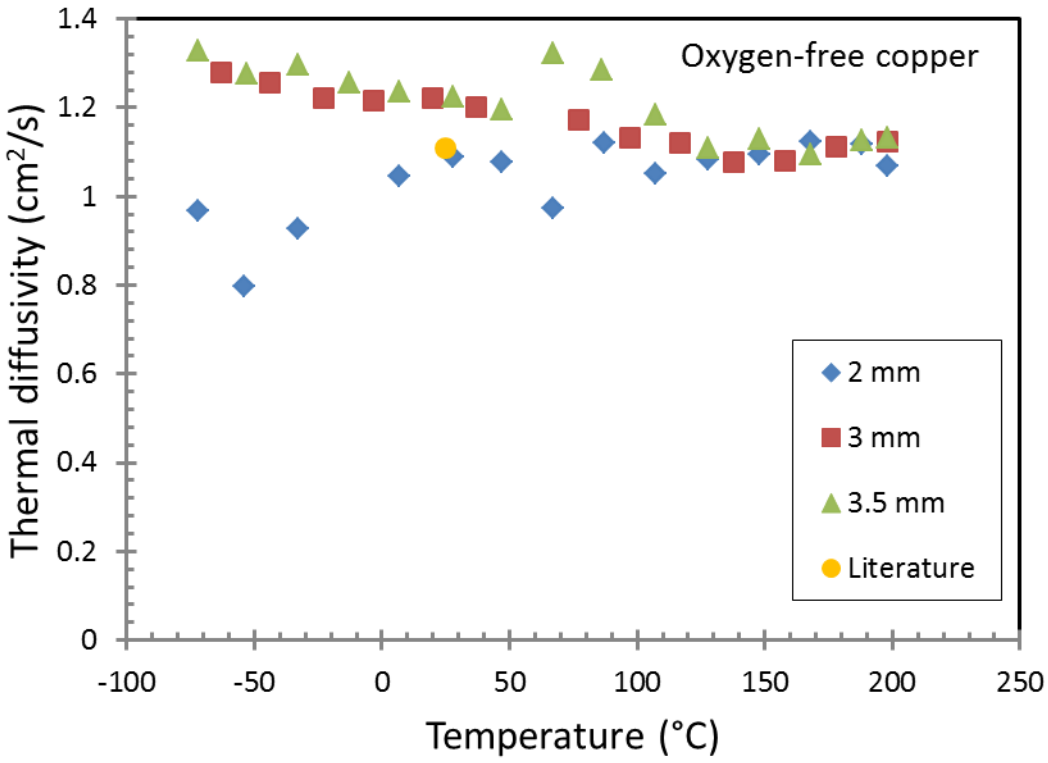

Figure 15. The measured thermal diffusivity data of three oxygen-free copper discs from 75°C to 200°C.

D. Thermal Conductivity of oxygen-Free Copper

When the measured thermal diffusivity data from Figure 15 are multiplied with the density and heat capacity data of copper from literature according to equation 2, the results of thermal conductivity are plotted on Figure 16, together with data reported in the literature (yellow dots). The results show our measurements, particular with 3 mm thick oxygen-free copper disc, are in good agreement with the literature data. The slightly higher thermal conductivity of our samples might be attributed to the higher purity of our specimens as these samples are free of oxygen in the crystalline lattice that can effectively reduce thermal impedance in copper. Once again, we can see the propagation of the "finite pulse width effect" from the thermal diffusivity measurement in the thinnest sample (L = 2 mm), resulting in a large data scattering of calculated thermal conductivity.

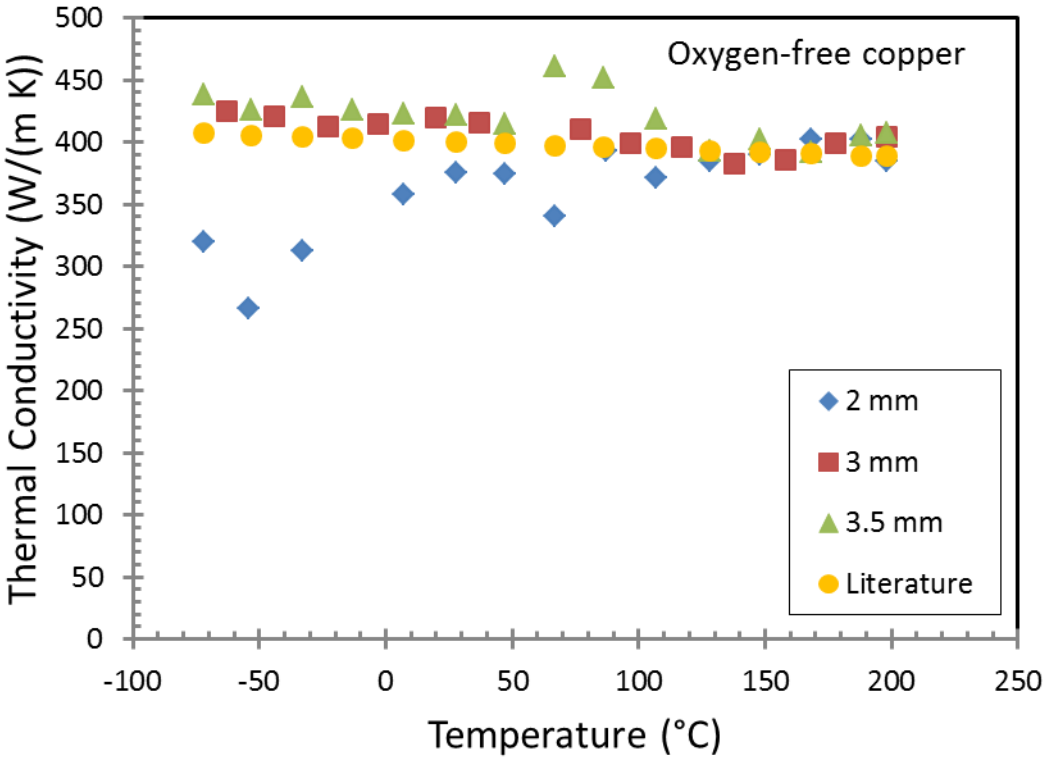

Figure 16. The measured thermal conductivity from three different sample thicknesses of oxygen-free copper specimens. The yellow dots are the thermal conductivity data of copper collected in the literature.

E. Heat Losses

Figure 17 provides additional evidence to support the heat loss argument due to sample configuration in the sample holder. These data were collected from the 3 mm thick diamond-copper sample in two possible different configurations where one configuration might have more edge surface in direct contact with the sample holder than the other. As mentioned in section 3.4,

the measured thermal diffusivity for run # 454 is higher than run #455 and run #456. The data in these runs are not scattered but show a monotonic decrease as temperature rises and the last two measurements are almost identical. Closely examining the temporal responses close to room temperature from run #454 and run #456, we find that even Run #464 was taken at a slightly lower temperature, it has a higher temperature rise than run #466, a slightly shorter rise time (or $t_{1/2}$, see insert figure), therefore, showing a higher thermal diffusivity. In addition, the temporal response for run #466 at the tail (t > 1 sec) drops faster than run #464, indicating a higher heat loss by conduction. Although these observations may be suggestive, the measured thermal diffusivity should not vary more than the system error (i.e., 4%) unless there is a heat loss during measurement.

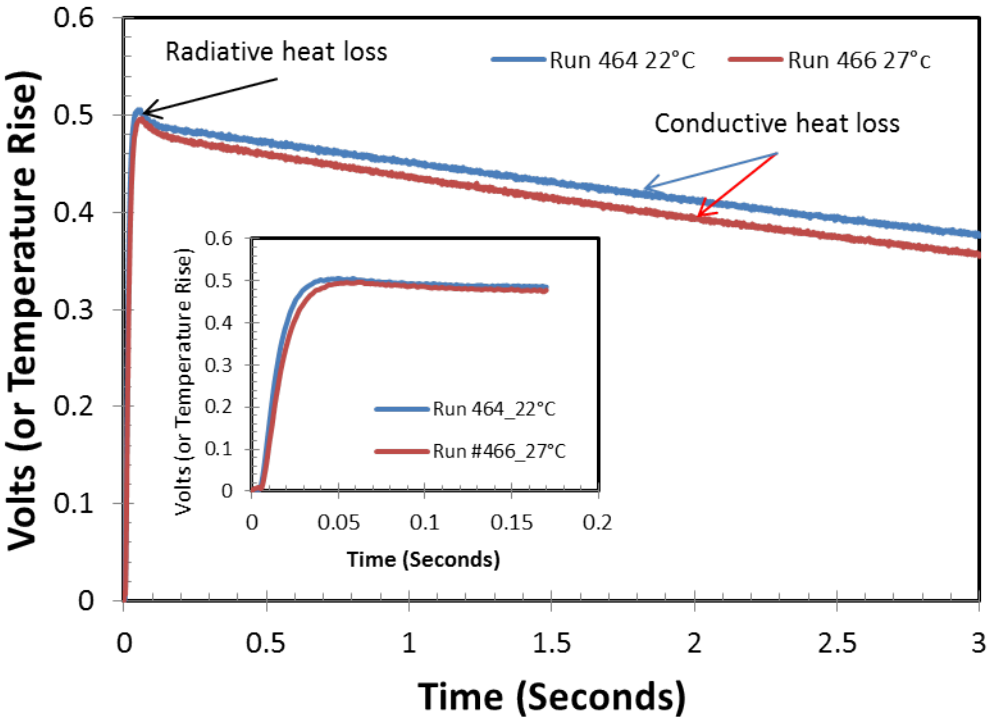

Figure 17. A comparison of the temporal responses form run #464 and run #466 of the 3 mm copper-diamond specimen. After reaching the peak temperature, the negative slope of run #466 is greater than run #464 suggesting there is more heat loss when the sample is at run #466 configuration than it is at run #464.

F. Material Specifications (MetGRAF^{Tm} Product)

Metal Matrix Composites for Thermal Management

Low expansion, lightweight, high thermal conductivity aluminum and copper graphite composites for heat sink, base plate, thermal spreader, and packaging applications.

	MetGraf 4-230	MetGraf 7-200	Cu MetGraf 7-300	Cu MetGraf 4-280
Matrix Alloy	Al	Al	Cu	Cu
TC (W/mK)				
In Plane (x-y)	220-230	185-200	285-300	265-280
Thickness (z)	120	125	210	200
Cp (J/g-K)	0.852	0.879	0.433	0.448
CTE (Avg. -55°C to 125°C ppm/C)				
In Plane (x-y)	4	7	7	4
Thickness (z)	24	24	16	16
Tensile Strength (ksi)				
In Plane (x-y)	15	13.5	10	9.9
Thickness (z)	–	5.5	5	
Compressive Strength (ksi)	29.4	29.4	28.5	
Yield Strength (ksi In Compression)	15.9	15.9	12.2	
Young's Modulus (msi)	14.3	12.9	11.0	10.4
Flexure Strength (ksi)	27	23	23	
Electrical Resistivity (µ·ohm·cm)	–	6.89	4.36	
Hardness (Rockwell E)	–	60-80	-	
Density (g/cc)	2.40	2.46	6.07	5.5
Plating	Ni, Au, Ag	Ni, Au, Ag	Ni, Au, Ag	Ni, Au, Ag

DISTRIBUTION

1	MS0348	Rickard T Knudson	05352 (electronic copy)
1	MS0348	Chris L. Gibson	05352 (electronic copy)
1	MS0348	John C, Moser III	05352 (electronic copy)
1	MS0348	John L. Williams	05353 (electronic copy)
1	MS0525	Gregory C. Frye-Mason	02632 (electronic copy)
1	MS0525	Thomas P. Swiler	02632 (electronic copy)
1	MS0958	Pin Yang	01816 (electronic copy)
1	MS0958	Christopher B. DiAntonio	02734 (electronic copy)
1	MS0958	Tom Chavez	01816 (electronic copy)
1	MS0959	Kenneth A. Peterson	01833 (electronic copy)
1	MS0959	Adrian L. Casias	01833 (electronic copy)
1	MS1070	Jordan E. Massad	01526 (electronic copy)
1	MS1349	Eric N. Coker	01815 (electronic copy)
1	MS1411	Paul G. Clem	01816 (electronic copy)
1	MS0899	Technical Library	09536 (electronic copy)


Sandia National Laboratories